Severe acute respiratory syndrome coronavirus (SARS-CoV) infection inhibition using spike protein heptad repeat-derived peptides

Berend Jan Bosch*, Byron E. E. Martina†, Ruurd van der Zee‡, Jean Lepault§, Bert Jan Haijema*, Cees Versluis¶, Albert J. R. Heck¶, Raoul de Groot*, Albert D. M. E. Osterhaus†, and Peter J. M. Rottier*‖

Divisions of *Virology and ‡Immunology, Department of Infectious Diseases and Immunology, Faculty of Veterinary Medicine, and Institute of Biomembranes, Utrecht University, 3584 CL Utrecht, The Netherlands; †Department of Virology, Erasmus Medical Centre, 3015 GE Rotterdam, The Netherlands; §Virologie Moléculaire et Structurale, Centre National de la Recherche Scientifique, 91190 Gif-sur-Yvette, France; and ¶Department of Biomolecular Mass Spectrometry, Bijvoet Centre for Biomolecular Research and Utrecht Institute for Pharmaceutical Sciences, 3584 CA Utrecht, The Netherlands

Edited by Peter S. Kim, Merck Research Laboratories, West Point, PA, and approved April 12, 2004 (received for review January 26, 2004)

The coronavirus SARS-CoV is the primary cause of the life-threatening severe acute respiratory syndrome (SARS). With the aim of developing therapeutic agents, we have tested peptides derived from the membrane-proximal (HR2) and membrane-distal (HR1) heptad repeat region of the spike protein as inhibitors of SARS-CoV infection of Vero cells. It appeared that HR2 peptides, but not HR1 peptides, were inhibitory. Their efficacy was, however, significantly lower than that of corresponding HR2 peptides of the murine coronavirus mouse hepatitis virus (MHV) in inhibiting MHV infection. Biochemical and electron microscopical analyses showed that, when mixed, SARS-CoV HR1 and HR2 peptides assemble into a six-helix bundle consisting of HR1 as a central triple-stranded coiled coil in association with three HR2 α-helices oriented in an antiparallel manner. The stability of this complex, as measured by its resistance to heat dissociation, appeared to be much lower than that of the corresponding MHV complex, which may explain the different inhibitory potencies of the HR2 peptides. Analogous to other class I viral fusion proteins, the six-helix complex supposedly represents a postfusion conformation that is formed after insertion of the fusion peptide, proposed here for coronaviruses to be located immediately upstream of HR1, into the target membrane. The resulting close apposition of fusion peptide and spike transmembrane domain facilitates membrane fusion. The inhibitory potency of the SARS-CoV HR2-peptides provides an attractive basis for the development of a therapeutic drug for SARS.

Severe acute respiratory syndrome (SARS) is a new, often fatal disease in humans for which as yet no cure exists. It is caused by a novel coronavirus, SARS-CoV, that probably originated from a wild animal reservoir. An attractive approach to interfere with SARS disease progression focuses on one of the earliest processes of infection, by blocking the fusion process that mediates the delivery of the viral genome into the host cell. When applied at an early stage, such an approach would prevent or reduce the spread of the infection within and beyond the respiratory organs. Coronaviruses are enveloped viruses both the receptor binding and the membrane fusion process of which are mediated by the spike (S) membrane glycoprotein (reviewed in ref. 1). We have shown recently that murine coronavirus (MHV) uses a spike-mediated membrane fusion mechanism that has many similarities to that of so-called class I virus fusion proteins (2).

Class I virus fusion proteins, like the influenza virus hemagglutinin, the HIV-1 *env* and the paramyxovirus F protein, have a number of common structural features. They are type I membrane glycoproteins that fold into trimers and contain a protease cleavage site, a fusion peptide and at least two heptad repeat regions, one of which (here designated as HR1) is located downstream and in the vicinity of the fusion peptide, whereas the other (HR2) usually occurs adjacent to the transmembrane domain (3). The fusion proteins acquire a metastable state upon cleavage by cellular proteases. After binding of virus to the receptor or because of protonation during endocytosis, class I fusion proteins proceed through a series of conformational changes to mediate membrane fusion with the host cell. Initially, the fusion peptide located at or close to the N terminus of the membrane-anchored subunit becomes exposed and can insert into the cellular membrane. This is followed by further rearrangements within the protein trimer resulting in the formation of a six-helix bundle. In this structure, a homotrimeric coiled coil formed by HR1 is surrounded by three HR2 helices that pack against the HR1 coiled coil in an antiparallel manner. In the full-length protein, such a conformation leads to a close apposition of the fusion peptide (N-terminally of HR1), inserted in the cellular membrane, and the viral transmembrane segment (C-terminally of HR2), facilitating membrane fusion (for a review on class I fusion protein mechanism, see ref. 4).

The coronavirus spike protein has striking similarities with class I fusion proteins. It is a type I membrane protein that oligomerizes into trimers (5), although dimers of the spike protein have also been reported (6). The N-terminal half of the protein (S1) contains the receptor-binding domain (7, 8), whereas the C-terminal half (S2) is the membrane-anchored membrane fusion subunit (9). Similar to class I fusion proteins, the S2 protein contains two heptad repeat regions of which one (HR2) is located close to the transmembrane anchor, the other (HR1) is ≈170 residues upstream of it (10). Despite these strong similarities to class I virus fusion proteins, coronavirus spike proteins have several characteristics that set them apart. First, unlike class I fusion proteins, cleavage is not essential for coronavirus infection; rather, group 1 coronaviruses are not cleaved at all. Second, although class I fusion proteins carry their fusion peptide at or close to the N terminus of the membrane anchored membrane fusion subunit, no such hydrophobic peptide occurs in this region of (cleaved) coronavirus spike proteins. Although the precise location of the fusion peptide still needs to be determined, it is clear that membrane fusion is mediated by an internal fusion peptide.

Here we have explored the potential of HR peptides as therapeutic agents against SARS. As has been described for retrovirus, paramyxovirus, and coronavirus fusion proteins (2, 11–16), peptides derived from the HR2 domain can inhibit virus infection, most likely by interfering with six-helix bundle formation, a process essential to drive the membrane fusion reaction and, thus, to initiate infection. For HIV-1, this has led to the development of peptide

This paper was submitted directly (Track II) to the PNAS office.

Abbreviations: HR, heptad repeat; SARS, severe acute respiratory syndrome; MHV, murine coronavirus; IMDM, Iscove's modified Dulbecco's medium; O/N, overnight; ESI-TOF, electrospray ionization time-of-flight.

‖To whom correspondence should be addressed. E-mail: p.rottier@vet.uu.nl.

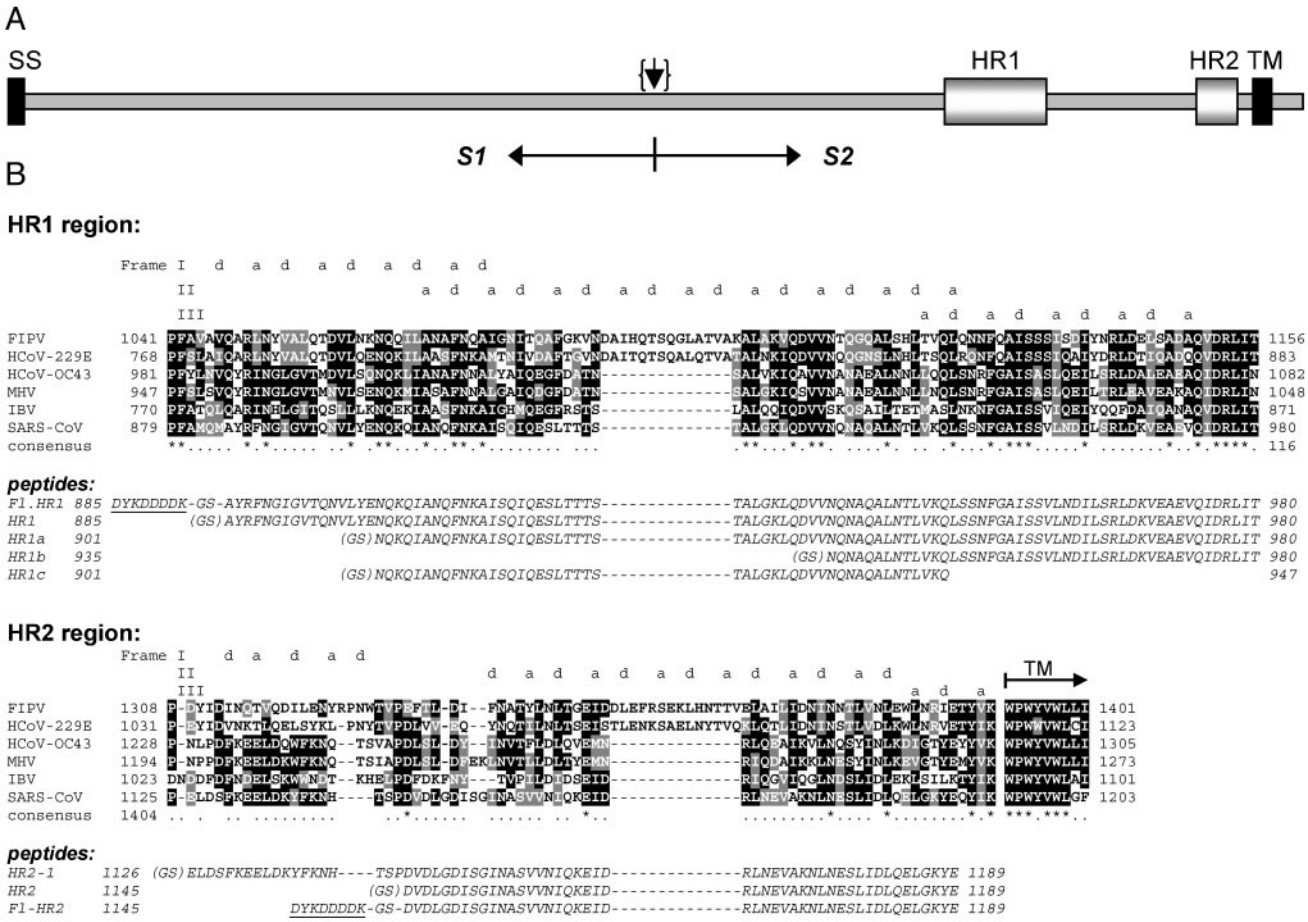

Fig. 1. (*A*) Schematic representation of the coronavirus spike protein structure. The glycoprotein has an N-terminal signal sequence (SS) and a transmembrane domain (TM) close to the C terminus. Group 2 and 3 coronavirus spike proteins are proteolytically cleaved (arrow) in an S1 and an S2 subunit, which are noncovalently linked. S2 contains two heptad repeat regions (shaded bars), HR1 and HR2, as indicated. (*B*) CLUSTALW multiple sequence alignment of coronavirus spike proteins. Shown is the alignment of the HR1 and HR2 domains of the recently identified SARS-CoV (strain TOR2) with those of the group 1 coronaviruses FIPV (feline infectious peritonitis virus strain 79–1146) and HCoV-229E (human coronavirus strain 229E), the group 2 coronaviruses MHV-A59 (mouse hepatitis virus strain A59) and HCoV-OC43 (human coronavirus strain OC43), and the group 3 coronavirus IBV (infectious bronchitis virus strain Beaudette) (GenBank accession nos. P59594, VGIH79, VGIHHC, P11224, CAA83661, and P11223, respectively). Dark shading marks sequence identity, whereas lighter shading represents sequence similarity. The alignment shows a remarkable insertion of exactly two heptad repeats (14 aa) in both HR1 and HR2 of HCV-229E and FIPV, a characteristic of all group 1 viruses. The predicted hydrophobic heptad repeat ''a'' and ''d'' residues are indicated above the sequence. Asterisks denote conserved residues, dots represent similar residues. The amino acid sequences of the HR1-derived peptides HR1, HR1a, HR1b, HR1c, and a FLAG-tagged HR1 (Fl.HR1) and of the HR2 derived peptides HR2, HR2-1 and a FLAG-tagged HR2 (Fl.HR2) of SARS-CoV used in this study are presented in italics below the alignments. N-terminal glycine and serine residues derived from the thrombin proteolytic cleavage site of the GST fusion protein are in parentheses.

inhibitors, one of which has recently been licensed as a drug against AIDS. Our results demonstrate that SARS-CoV HR peptides assemble into a rod-like complex composed of an inner α-helical HR1 homotrimer packed with three HR2 α-helices oriented in an antiparallel fashion. SARS-CoV infection of Vero cells appeared to be markedly inhibited, in a concentration-dependent manner, by HR2-derived peptides, although the effect was clearly less than that of corresponding HR2 peptides on MHV infection of murine cells. As judged from the different thermal stabilities of the HR1–HR2 complexes, this difference is probably explained by a relatively weaker interaction strength of the SARS-CoV peptides.

Materials and Methods

Inhibition of SARS-CoV Infection. Construction of bacterial expression vectors, expression and purification of the peptides have been described (2) (see *Supporting Text* and Table 2, which are published as supporting information on the PNAS web site). Vero 118 cells were maintained in Iscove's modified Dulbecco's medium (IMDM; BioWhittaker) supplemented with 5% FBS (Greiner, Kremsmuenster, Germany), penicillin (100 units/ml), streptomycin (100 μg/ml), and 2 mM L-glutamine. The initial experiments were performed on Vero 118 cells grown on cover slips in 24-well plates (2×10^5 cells per well) at 37°C. Cells were inoculated with SARS-CoV (strain 5688, fourth passage; ref. 17) (multiplicity of infection = 0.5) in the presence of HR peptide at different concentrations. After 1 h, the inoculum was removed, the cells were washed twice with IMDM, and the cells were overlaid with IMDM containing 5% FBS and the peptide at similar concentration as used in the inoculum. After overnight (O/N) incubation, cells were washed twice with PBS and fixed by 70% ethanol for 30 min at −20°C. After washing the plates twice with PBS and twice with bidest, the cover slips were incubated for 1 h at 37°C with a polyclonal serum (1:100) obtained from a convalescent SARS patient. FITC-labeled rabbit-anti-human IgG (Dako) was used as a conjugate in a 1:80 dilution. Pictures of FITC fluorescent cells were taken by using a MC80 camera mounted on an Axioskop microscope (Zeiss).

The second set of inhibition experiments was performed on Vero 118 cells in 96-well plates (10^4 cells per well). Cells were inoculated

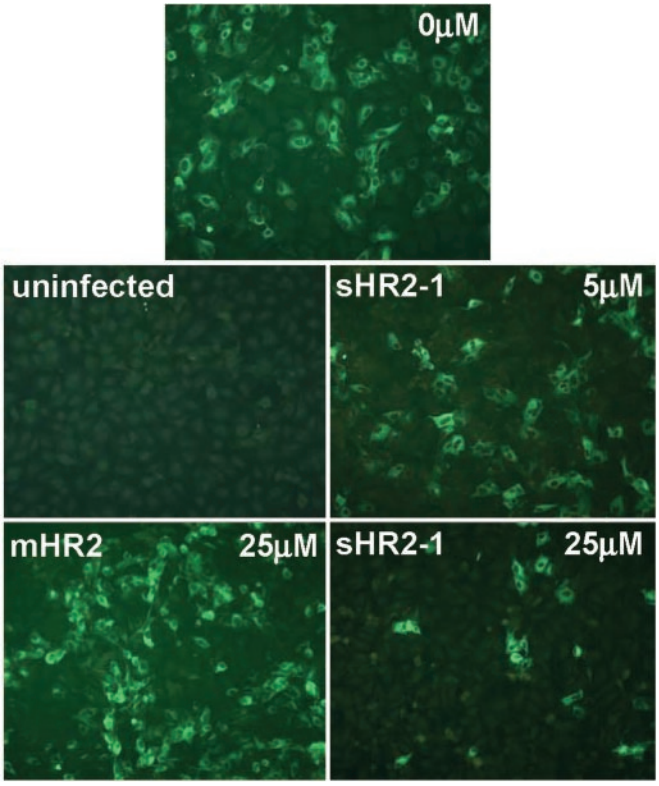

Fig. 2. Inhibition of SARS-CoV infection by HR peptides. (*A*) VERO cells were mock infected or infected with SARS-CoV (multiplicity of infection = 0.5) in the presence of the HR2-1 peptide (sHR2-1) at concentrations of 0, 5, or 25 μM and incubated in medium containing the same concentration of peptide. An infection in the presence of peptide (25 μM) corresponding to the HR2 domain of MHV (mHR2) was taken along as a negative control. At 16 h after infection, cells were fixed, and SARS-CoV-positive cells were visualized by immunofluorescence staining.

in triplicate with 100 $TCID_{50}$ of SARS-CoV in the presence of various peptide concentrations, ranging from 0.4 to 50 μM, for 1 h at 37°C in a CO_2 incubator. Cells were then washed twice with IMDM, and the medium was replaced with IMDM containing 5% FBS. After incubation for 9 h, plates were washed twice with PBS and fixed by 4% formaldehyde for 15 min and 70% ethanol plus 0.5% H_2O_2 for 15 min at room temperature. After washing the plates twice with PBS plus 0.5% Tween 20 and twice with PBS, the fixed and permeabilized cells were incubated for 1 h at 37°C with a polyclonal antiserum obtained from SARS-CoV-infected ferrets (1:40) (18). Horseradish peroxidase (HRP)-labeled goat-anti-ferret antibodies (Dako) were used as a conjugate in a 1:50 dilution. Reaction was developed with 3-amino-9-ethylcarbazole (AEC; Sigma) according to the manufacturer's instructions. Inhibition of MHV by HR peptides was tested as described above but using LR7 cells (19) rather than VERO 118 cells. Immunoperoxidase (IPOX) detection of MHV-positive cells was carried out by using a rabbit polyclonal antibody against MHV (1:300) (20) in combination with a HRP swine-anti rabbit antibody (1:300) (Dako). Experiments were performed in triplicate and carried out in duplo. Infected cells were counted by using the light microscope, and the effective peptide concentration at which 50% of the infection was inhibited (EC_{50}) was calculated by fitting the HR peptide inhibition data to a Langmuir function [normalized number of infected cells = $1/(1 + [\text{HR peptide}]/IC_{50})$].

Size Exclusion HPLC. Peptides HR1 and HR2 and a preincubated equimolar mix of HR1 and HR2 were purified by size exclusion HPLC on a Superdex 75 PC 3.2/30 column (Amersham Pharmacia) using 200 mM ammonium acetate (pH 5.0) as a running buffer.

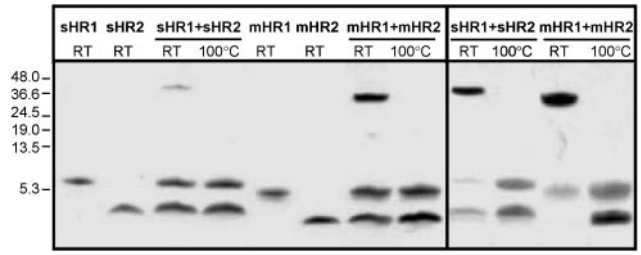

Fig. 3. Complex formation of SARS-CoV HR1 and HR2 peptides. Comparison of SARS-CoV and MHV. HR1 and HR2 peptides on their own or as a preincubated equimolar mixture were subjected to 15% Tricine SDS/PAGE. Just before loading onto the gel, some samples were heated at 100°C. In *Left* and *Right*, complex formation was analyzed after a 3 h and an O/N incubation, respectively.

Nano Electrospray Ionization Time-of-Flight Mass Spectrometry (Nano-ESI-TOF). Peak fractions collected after size exclusion HPLC were analyzed by nano-ESI-TOF mass spectrometry (Micromass LC-T, Manchester, U.K.) at a concentration of 10 μM in 200 mM ammonium acetate (pH 5.0). The potential between the nano-ESI needle and the sample cone was set at 1,300 V, and the cone voltage was 30 V. Nano-ESI needles were made from borosilicate glass capillaries with a P-97 puller (Sutter Instruments, Novato, CA). Needles were gold-coated by using an Edwards Scancoat Six sputter coater (Crawley, U.K.).

Temperature Stability of SARS-CoV and MHV HR1–HR2 Complex. Equimolar mixes of HR1 and HR2 peptides (100 μM each) of SARS-CoV and MHV were incubated in parallel at room temperature for 3 h, to allow HR1–HR2 complex formation. Twenty-five microliters of each mix was pooled, and an equal volume of 2× Tricine sample buffer (21) was added. The mixtures were either left at room temperature or heated for 5 min at different temperatures and subsequently analyzed by SDS/PAGE in 15% Tricine gel (21).

Proteinase K Treatment. Stock solutions (250 μM) of the peptides HR1a, HR1c, and HR2 in water were diluted to 100 μM in 50 mM Tris, pH 7.0. Peptides on their own (100 μM) or HR1–HR2 mixtures (100 μM each) preincubated for 3 h at 37°C were subjected to proteinase K digestion (1% wt/wt, proteinase K/peptide) for 2 h at 4°C. Protease resistant fragments were separated and purified by reverse-phase HPLC and characterized by mass spectrometry.

Results

HR Regions in the SARS-CoV Spike Protein. As shown for other coronaviruses (10), two HR regions, identified by their characteristic seven-residue periodicity and their alignment with similar regions in other coronavirus spike proteins, are present in the C-terminal S2 domain of the SARS-CoV spike protein (Fig. 1). One region (HR2) is located adjacent to the transmembrane domain, the other (HR1) is ≈170 residues upstream. In all coronaviruses, HR1 is consistently larger than HR2. However, the feline infections peritonitis virus (FIPV) and HCoV-229E coronaviruses show a remarkable insertion of two heptad repeats (14 aa) in both HR regions (2, 10). This insertion is lacking in the SARS-CoV HR regions. The HR2 region of SARS-CoV contains three conserved *N*-glycosylation sites (N-X-S/T; Fig. 1*B*).

HR Peptides and Their Infection Inhibitory Activities. HR regions play an important role in the membrane fusion process (2, 4). To

Table 1. Amino acid sequences and EC_{50} values of HR2- and HR1-derived peptides

Peptide	Amino acid sequence	$EC_{50} \pm SD$, μM SCV	$EC_{50} \pm SD$, μM MHV
HR2			
sHR2-1	ELDSPKEELDKYFKNHTSPDVDLGDISGINASVVNIQKEIDRLNEVAKNLNESLIDLQELGKYE	43 ± 6.4	>50
sHR2-2	PKEELDKYFKNHTSPDVDLGDISGINASVVNIQKEIDRLNEVAKNLNESLIDLQELGKYE	24 ± 2.8	ND
sHR2-3	LDKYFKNHTSPDVDLGDISGINASVVNIQKEIDRLNEVAKNLNESLIDLQELGKYE	>50	ND
sHR2-4	FKNHTSPDVDLGDISGINASVVNIQKEIDRLNEVAKNLNESLIDLQELGKYE	>50	ND
sHR2-5	TSPDVDLGDISGINASVVNIQKEIDRLNEVAKNLNESLIDLQELGKYE	>50	ND
sHR2-6	VDLGDISGINASVVNIQKEIDRLNEVAKNLNESLIDLQELGKYE	>50	ND
sHR2-7	DISGINASVVNIQKEIDRLNEVAKNLNESLIDLQELGKYE	>50	ND
sHR2-8	ELDSFKEELDKYFKNHTSPDVDLGDISGINASVVNIQKEIDRLNEVAKNLNESLIDLQELGKYEQYIK	17 ± 3.0	ND
sHR2-9	ELDSFKEELDKYFKNHTSPDVDLGDISGINASVVNIQKEIDRLNEVAKNLNESLIDLQEL	34 ± 4.0	ND
sHR2-10	ELDSPKEELDKYFKNHTSPDVDLGDISGINASVVNIQKEIDRLNEVAKNLNESLID	>50	ND
mHR2	DLSLDFEKLNVTLLDLTYEMNRIQDAIKKLNESYINLKE	>50	0.9 ± 0.1
HR1			
sHR1	AYRFNGIOVTQNVLYE-NQKQIANQFNKAISQIQESLTTTSTALGKLQDVVNQNAQALNTLVKQLSSNFGAISSVLNDILSRLDKVEAEVQIDRLIT	>50	ND
sHR1a	NQKQIANQFNKAISQIQESLTTTSTALGKLQDVVNQNAQALNTLVKQLSSNFGAISSVLNDILSRLDKVEAEVQIDRLIT	>50	ND
sHR1b	NQKQIANQFNKAISQIQESLTTTSTALGKLQDVVNQNAQALNTLVKQLSSNFGAISSVLNDILSRLDKVEAEVQIDRLIT	>50	ND
sHR1c	NQNAQALNTLVKQLSSNFGAISSVLNDILSRLDKVEAEVQIDRLIT	>50	ND

Shown are amino acid sequences of HR2- and HR1-derived peptides of SARS-CoV (SCV) and MHV and their EC_{50} values as determined in a 96-well format infection inhibition assay. >50 μM, <50% inhibition was observed at 50 μM (the highest concentration tested) or no inhibition at all, as was the case for the mHR2 peptide and the sHR2–1 peptide when tested against SARS-CoV and MHV infection, respectively.

evaluate this role in the case of SARS-CoV, peptides corresponding to the HR regions were prepared by using the bacterial GST expression system and purified to homogeneity by using reverse-phase HPLC, and their molecular masses were verified by mass spectrometry. Peptides were subsequently tested for their inhibitory potency in an infection inhibition assay. VERO cells were inoculated with SARS-CoV (multiplicity of infection = 0.5) in the absence or presence of different concentrations of a particular peptide, and the extent of infection was evaluated by using an indirect immunofluorescence assay. As shown in Fig. 2 for one of the initial peptides tested, HR2-1, a clear concentration-dependent inhibition of SARS-CoV infection was observed. This effect was sequence specific, as no inhibition was seen with a corresponding peptide derived from the HR2 region of MHV (mHR2), known to block MHV infection (2).

To study the sequence dependence and to optimize the efficacy of the inhibition, we prepared two sets of peptides, the sequences of which are compiled in Table 1. One set consisted of HR2-1 based peptides: a series of peptides with increasing four-residue N-terminal truncations (HR2-2 to HR2-7), one peptide with a four-residue C-terminal extension (HR2-8), and two peptides with four- and eight-residue C-terminal truncations (HR2-9 and HR2-10, respectively). The other set consisted of peptides corresponding to the HR1 region, with peptide HR1 comprising almost the entire HR region, and peptides HR1a-c representing N- and C-terminal truncations thereof. These peptides were tested similarly, but the infection levels were now determined in a technically different format, by using immune peroxidase staining followed by a readout of the percentage of infected cells. Table 1 shows the EC_{50} values obtained, i.e., the concentrations calculated to cause a 50% reduction of infection. It is clear that slight truncations at either side of the HR2-1 peptide are tolerated without loss of inhibitory activity. Actually, shortening HR2-1 just by four residues at the N-terminal (HR2-2) or the C-terminal side (HR2-9) resulted in significantly enhanced inhibition. C- or N-terminal truncations of the sHR2-1 peptide by >4 aa resulted in a decrease of infection inhibition. The most effective peptide of the panel was HR2-8, which carried the C-terminal four-residue extension. It had an EC_{50} value of 17 μM. The inhibition efficiency of this peptide was clearly lower than that of an HR2 peptide of MHV, mHR2, which had an EC_{50} value of 0.9 μM when tested in the MHV infection system. Of the panel of HR1-derived peptides, none showed any measurable inhibitory effect on SARS-CoV infection.

HR1–HR2 Complex Formation. We have previously shown that the HR1 and HR2 peptides of the MHV spike protein, when mixed together, assemble into an oligomeric complex that is resistant to 2% SDS (2). Using the same approach, we observed that the HR1 and HR2 peptides of the SARS-CoV spike protein behave in a similar manner. As shown in Fig. 3 for equimolar mixtures of similar HR peptides from both viruses, SDS-stable oligomeric complexes are formed that dissociate upon heating. Complex formation was limited after 3 h, but almost complete after O/N incubation (Fig. 3 *Left* and *Right*, respectively). Upon heating, the complexes dissociated, giving rise to the individual subunits HR1 and HR2 (Fig. 3 *Right*). The presence of both HR1 and HR2 in the complex was confirmed by using FLAG-tagged HR peptides by SDS/PAGE analysis of mixtures of tagged and nontagged HR peptides (see Fig. 6, which is published as supporting information on the PNAS web site).

Stoichiometry of Peptides in the HR1–HR2 Complex. The stoichiometry of peptides in the HR1–HR2 complex was analyzed by nano-ESI-TOF mass spectrometry, a convenient method to study noncovalent macromolecular protein complexes (22). Peptides HR1 and HR2 and an O/N-preincubated equimolar mixture of HR1 and HR2 were subjected to size-exclusion HPLC (Fig. 4*A*). The HR1–HR2 complex ran as a single peak, indicating complete complex formation, and eluted from the column before the HR1 and HR2 peptides. The HR1 and HR2 peaks and the HR1–HR2 complex peak were analyzed by nano-ESI-TOF (Fig. 4*B*). The observed molecular mass of the HR1 (10710.8 Da) and HR2 (5129.6 Da) peptides corresponded to their calculated masses (calculated Mw: HR1, 1,0711.0 Da; HR2; 5,129.6 Da). The HR1–HR2 complex produced m/z values of 2,796.4, 2,971.1, 3,169.2, and 3,395.6 representing the 17+, 16+, 15+, and 14+ protonated forms, respectively, of the complex with a convoluted mass of 4,7524.4 Da. The observed mass corresponds almost exactly to the calculated mass of a complex consisting of three HR1 peptides and three HR2 peptides (calculated Mw, 47,521.8 Da). The stochiom-

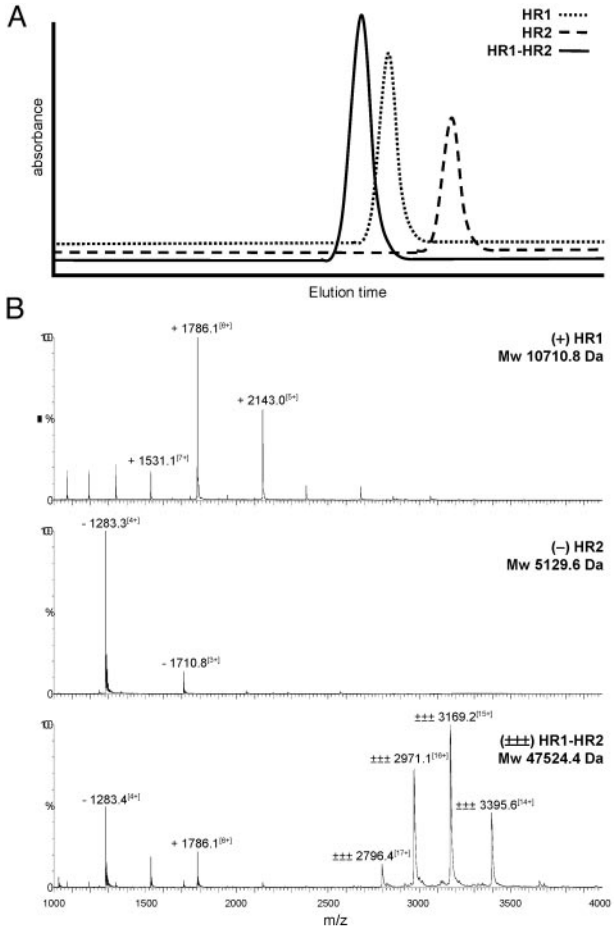

Fig. 4. Stoichiometry of peptides in HR1–HR2 complexes. (*A*) Size-exclusion HPLC elution profile of the HR1 peptide (dotted line), HR2 peptide (dashed line), and an O/N preincubated equimolar mix of the HR1 and HR2 peptides (solid line). (*B*) Nano-ESI-TOF mass spectrum of the HR1 and HR2 peptides and of the HR1–HR2 complex. m/z values of the peaks of the HR1 (+; *Top*), the HR2 peptide (−; *Middle*) or the HR1–HR2 peptide complex (±±±; *Bottom*) are indicated, with the charge state assignment in brackets. The convoluted average molecular mass (Mw) of the HR1 and HR2 peptides and of the HR1–HR2 peptide complex are indicated as well. Peaks corresponding to the HR1 and HR2 monomers are visible in the lower m/z range of the spectrum of the complex, indicating that a fraction of it dissociated during the procedure.

etry of the peptides in the complex was independently confirmed by using FLAG-tagged HR peptides by SDS/PAGE analysis of mixtures of tagged and nontagged HR peptides (see Fig. 6).

Temperature Stability of HR1–HR2 Complex. The stability of the SARS-CoV HR1–HR2 complex to temperature dissociation was assessed in comparison to that of the corresponding MHV complex. Equal amounts of both complexes were combined, and the solution was adjusted to 1× Tricine sample buffer. Equal samples were taken, incubated in parallel for 5 min at different temperatures, and subsequently analyzed by 10% Tricine SDS/PAGE (Fig. 5). Because of their distinct electrophoretic mobilities, the SARS-CoV and MHV complexes could clearly be distinguished, allowing the direct comparison of their temperature sensitivity. Surprisingly, the SARS-CoV HR complex appeared to be significantly less stable than that of MHV, with dissociation occurring at 70°C and 90°C, respectively.

Structural Analysis of HR1 and HR2 Peptides and of the HR1–HR2 Complex. Analysis using circular dichroism revealed that peptides HR1 and HR2 and the HR1–HR2 complex were highly α-helical,

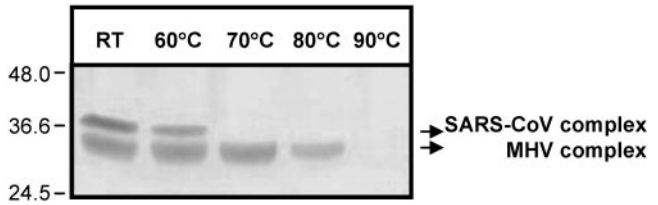

Fig. 5. Comparative temperature stabilities of HR1–HR2 complexes of SARS-CoV and MHV. Equal amounts of SARS-CoV and MHV HR1–HR2 complexes were pooled, subsequently incubated for 5 min at the indicated temperatures in 1× Tricine sample buffer and analyzed directly by SDS/PAGE in a 15% Tricine gel. Positions of the HR1–HR2 complex of SARS-CoV and MHV are indicated on the right, and the molecular mass markers are indicated at the left.

with calculated helical content values of 85% (HR1), 81% (HR2), and 88% (HR1–HR2) (see Fig. 7, which is published as supporting information on the PNAS web site). By electron microscopy the HR1–HR2 complex appeared as a rod-like structure with a length of 14.4 nm (±2.4 nm), similar to the length observed earlier for the MHV HR1–HR2 complex. Similar rod-like structures were seen in samples containing just the HR1 peptide (14.3 ± 2.4 nm) not with the HR2 peptide only, confirming that HR1 does assemble into a, presumably homotrimeric, coiled coil on its own (see Fig. 8, which is published as supporting information on the PNAS web site). Strongly folded protein structures are often resistant to proteolytic degradation. When we used limited proteinase K digestion in combination with reverse-phase HPLC and mass spectrometry analysis, we observed that HR2 was completely degraded by the enzyme, whereas only the C-terminal six residues of the HR1a peptide were sensitive to proteinase K. When a mixture of the two peptides was analyzed, the HR2 peptide was entirely protected from proteolytic breakdown. A similar analysis carried out with a C-terminally truncated version of HR1a, HR1c, revealed that now the N terminus of HR2 was proteolytically degraded by 10 aa. These results indicate that in the HR1–HR2 complex, the HR1 and HR2 helices are oriented in an antiparallel fashion (for reverse-phase HPLC profiles and mass spectrometry analysis of the proteolytic fragments, see Fig. 9, which is published as supporting information on the PNAS web site).

Discussion

Our functional and biochemical analysis of the spike protein HR regions of SARS-CoV demonstrates that the virus uses a membrane fusion mechanism similar to that of class I fusion proteins. Peptides corresponding to the HR1 and HR2 domains were found to associate tightly into a complex, as has been observed previously for retrovirus, paramyxovirus, and coronavirus fusion proteins (2, 12, 23, 24). Analogous to the HIV-1 gp41, SV5 F, and HRSV F proteins (25–28), the HR1–HR2 complex was found to consist of a six-helix bundle that is composed of three HR1 and three HR2 α-helical peptides. Limited proteolysis analysis revealed that the HR1 and HR2 peptides in this complex are organized in an antiparallel orientation, presumably through interaction of the hydrophobic face of the HR2 helix with the hydrophobic groove in the HR1 coiled coil created by the mostly hydrophobic e and g residues of HR1. Formation of such an antiparallel six-helix bundle is essential for the membrane fusion process because it drives the close apposition of viral and cellular membrane. In the full-length spike protein the HR1–HR2 structure brings the fusion peptide, N-terminal of HR1, in close proximity to the transmembrane domain, C-terminal of HR2, thereby facilitating membrane fusion.

HR2-derived peptides, but not those derived from HR1, were able to inhibit SARS-CoV infection of Vero cells in a concentration-dependent manner. The effect is supposedly mediated by their competitive binding to the HR1 region of the SARS-CoV spike protein, thus blocking the formation of the six-helix bundle and,

consequently, membrane fusion (4). Of the limited number of HR2 derived peptides tested against SARS-CoV, the most effective one (HR2-8) was ≈20 times less potent than the corresponding HR2 peptide of MHV was in inhibiting MHV infection of murine cells (EC_{50} values of 17 and 0.9 μM, respectively). Although there are several possible reasons to explain this variation, such as a different route of virus entry, different membrane fusion kinetics, or a different accessibility of the target binding site, our comparison of the thermal stabilities of the fusion core complexes of the two viruses indicates that the difference has, at least in part, an energetic basis. The lower stability of the SARS-CoV six-helix bundle implies that the interaction strength between the HR1 and HR2 peptides is weaker, which correlates directly with a lower potency of the HR2 peptide in preventing the formation of this complex. The HR2-8 peptide will now be used as a lead for the further development of more effective SARS-CoV peptide inhibitors.

Interestingly, the HR1 peptide appeared to assemble into homotrimeric coiled coil structures in the absence of HR2. This was initially suggested by our observation that separately preincubated FLAG-tagged and nontagged HR1 peptides are unable to form mixed HR1–HR2 hexamers unless first dissociated by acetonitrile (see Fig. 6). It was also indicated by the resistance of HR1 to proteinase K and is consistent with the highly α-helical nature of the HR1 peptide. Under the electron microscope, the complexes were visible as rod-like structures similar in appearance and dimensions as the HR1–HR2 complexes. The formation of a protease-resistant homotrimeric coiled coil by the isolated HR1 peptides has been reported for the SV5 F protein (12) and for Moloney murine leukemia virus gp41 (29), but not for HIV-1 or SIV gp41 (23, 24), indicating the variation in stability of the HR1 core trimer among class I viral fusion proteins. There are no indications that a homotrimeric interaction between coronavirus HR1 regions already occurs in the native virion, i.e., before binding to the cell receptor. Rather, data indicate that interactions stabilizing the spike protein oligomer occur in the S1 part of the molecules (6).

A key element in all viral fusion proteins is the fusion peptide, a stretch of hydrophobic amino acids instrumental in connecting the viral and cellular membrane. The peptide occurs invariably upstream of the HR1 region of class I viral fusion proteins. No fusion peptide has as yet been identified in any of the coronavirus spike proteins. Significantly, unlike other class I fusion proteins, coronavirus spike proteins lack the cleavage requirement for virus infectivity. Although cleavage does not occur in many coronaviruses, including SARS-CoV (our unpublished data and ref. 30), its inhibition in viruses carrying a cleaveable spike protein, by using a furin inhibitor, appeared not to affect virus infectivity, as we demonstrated for MHV (31). Moreover, in these latter coronaviruses, the cleavage does not expose a hydrophobic sequence in the N-terminal domain of the membrane-anchored subunit. Consequently, coronavirus spike proteins use an internal fusion peptide and are not dependent on proteolytic activation, as are the vesicular stomatitis virus (VSV) G protein and class II fusion proteins such as the TBEV E and SFV E1 proteins. In an attempt to identify the coronavirus fusion peptide, we have used a transmembrane prediction program (TMAP), which predicts transmembrane domains (TM) in protein sequences by using multiple alignments. In the CLUSTALW alignment of nine coronavirus spike sequences, the TMAP program predicted three TM domains (see Fig. 10, which is published as supporting information on the PNAS web site). Besides the expected signal sequence (residues 1–15 in SARS-CoV S) and transmembrane anchor (residues 1195–1223), a hydrophobic region was predicted at the N terminus of the HR1 region (residues 858–886). Careful inspection of this sequence reveals that it has characteristics of a class II fusion peptide, notably the conserved proline residue (residue 879) and the high alanine and glycine content. This region has been noted earlier in a theoretical analysis of viral fusion proteins by Chambers *et al.* (32), but was dismissed later when mutation studies of the MHV spike protein pointed to another sequence (residues 971–989) as the likely fusion peptide (33). As we know now, this latter sequence is part of the HR1 domain, which explains the mutation results. Although the experimental evidence for the functioning of the putative fusion peptide immediately upstream of HR1 has yet to be provided, its location seems appropriate, because it would indeed become positioned adjacent to the transmembrane domain in the full-length protein after the rearrangements that give rise to the formation of the antiparallel six-helix bundle during the fusion reaction have taken place.

We thank Georgina Arron and Sylvia Reemers for their technical assistance and Gerard van Doornum for his supervision of the inhibition experiments.

1. Gallagher, T. M. & Buchmeier, M. J. (2001) *Virology* **279,** 371–374.
2. Bosch, B. J., van der Zee, R., de Haan, C. A. & Rottier, P. J. (2003) *J. Virol.* **77,** 8801–8811.
3. Lescar, J., Roussel, A., Wien, M. W., Navaza, J., Fuller, S. D., Wengler, G. & Rey, F. A. (2001) *Cell* **105,** 137–148.
4. Eckert, D. M. & Kim, P. S. (2001) *Annu. Rev. Biochem.* **70,** 777–810.
5. Delmas, B. & Laude, H. (1990) *J. Virol.* **64,** 5367–5375.
6. Lewicki, D. N. & Gallagher, T. M. (2002) *J. Biol. Chem.* **277,** 19727–19734.
7. Bonavia, A., Zelus, B. D., Wentworth, D. E., Talbot, P. J. & Holmes, K. V. (2003) *J. Virol.* **77,** 2530–2538.
8. Taguchi, F. (1995) *J. Virol.* **69,** 7260–7263.
9. Yoo, D. W., Parker, M. D. & Babiuk, L. A. (1991) *Virology* **180,** 395–399.
10. de Groot, R. J., Luytjes, W., Horzinek, M. C., van der Zeijst, B. A., Spaan, W. J. & Lenstra, J. A. (1987) *J. Mol. Biol.* **196,** 963–966.
11. Medinas, R. J., Lambert, D. M. & Tompkins, W. A. (2002) *J. Virol.* **76,** 9079–9086.
12. Joshi, S. B., Dutch, R. E. & Lamb, R. A. (1998) *Virology* **248,** 20–34.
13. Lambert, D. M., Barney, S., Lambert, A. L., Guthrie, K., Medinas, R., Davis, D. E., Bucy, T., Erickson, J., Merutka, G. & Petteway, S. R., Jr. (1996) *Proc. Natl. Acad. Sci. USA* **93,** 2186–2191.
14. Rapaport, D., Ovadia, M. & Shai, Y. (1995) *EMBO J.* **14,** 5524–5531.
15. Wild, C., Oas, T., McDanal, C., Bolognesi, D. & Matthews, T. (1992) *Proc. Natl. Acad. Sci. USA* **89,** 10537–10541.
16. Wild, C. T., Shugars, D. C., Greenwell, T. K., McDanal, C. B. & Matthews, T. J. (1994) *Proc. Natl. Acad. Sci. USA* **91,** 9770–9774.
17. Kuiken, T., Fouchier, R. A., Schutten, M., Rimmelzwaan, G. F., van Amerongen, G., van Riel, D., Laman, J. D., de Jong, T., van Doornum, G., Lim, W., *et al.* (2003) *Lancet* **362,** 263–270.
18. Martina, B. E., Haagmans, B. L., Kuiken, T., Fouchier, R. A., Rimmelzwaan, G. F., Van Amerongen, G., Peiris, J. S., Lim, W. & Osterhaus, A. D. (2003) *Nature* **425,** 915.
19. Kuo, L., Godeke, G. J., Raamsman, M. J., Masters, P. S. & Rottier, P. J. (2000) *J. Virol.* **74,** 1393–1406.
20. Rottier, P., Armstrong, J. & Meyer, D. I. (1985) *J. Biol. Chem.* **260,** 4648–4652.
21. Schagger, H. & von Jagow, G. (1987) *Anal. Biochem.* **166,** 368–379.
22. van Berkel, W. J., van den Heuvel, R. H., Versluis, C. & Heck, A. J. (2000) *Protein Sci.* **9,** 435–439.
23. Blacklow, S. C., Lu, M. & Kim, P. S. (1995) *Biochemistry* **34,** 14955–14962.
24. Lu, M., Blacklow, S. C. & Kim, P. S. (1995) *Nat. Struct. Biol* **2,** 1075–1082.
25. Weissenhorn, W., Dessen, A., Harrison, S. C., Skehel, J. J. & Wiley, D. C. (1997) *Nature* **387,** 426–430.
26. Chan, D. C., Fass, D., Berger, J. M. & Kim, P. S. (1997) *Cell* **89,** 263–273.
27. Baker, K. A., Dutch, R. E., Lamb, R. A. & Jardetzky, T. S. (1999) *Mol. Cell* **3,** 309–319.
28. Zhao, X., Singh, M., Malashkevich, V. N. & Kim, P. S. (2000) *Proc. Natl. Acad. Sci. USA* **97,** 14172–14177.
29. Fass, D. & Kim, P. S. (1995) *Curr. Biol.* **5,** 1377–1383.
30. Xiao, X., Chakraborti, S., Dimitrov, A. S., Gramatikoff, K. & Dimitrov, D. S. (2003) *Biochem. Biophys. Res. Commun.* **312,** 1159–1164.
31. de Haan, C. A. M., Stadler, K., Godeke, G.-J., Bosch, B. J. & Rottier, P. J. M. (2004) *J. Virol.*, in press.
32. Chambers, P., Pringle, C. R. & Easton, A. J. (1990) *J. Gen. Virol.* **71,** 3075–3080.
33. Luo, Z. & Weiss, S. R. (1998) *Virology* **244,** 483–494.